Available online at www.sciencedirect.com
SCIENCE DIRECT®
International Journal of Heat and Mass Transfer 49 (2006) 2840–2850
International Journal of HEAT and MASS TRANSFER
www.elsevier.com/locate/ijhmt

Control of temperature uniformity during the manufacture of stable thin-film photovoltaic devices

Chetan P. Malhotra [a,b,c], Roop L. Mahajan [b,*], W.S. Sampath [d], Kurt L. Barth [d], Robert A. Enzenroth [d]

[a] International Centre for Science and High Technology, Trieste, Italy
[b] Department of Mechanical Engineering, University of Colorado at Boulder, Campus Box 427, Boulder, CO 80309-0427, United States
[c] Tata Research Development and Design Centre, Pune 411 013, India
[d] Colorado State University, Fort Collins, CO 80521, United States

Received 16 August 2005; received in revised form 16 February 2006
Available online 24 April 2006

Abstract

The production of stable thin-film photovoltaic cells requires tight control of temperature uniformity within the glass substrates during the vacuum deposition process. Though traditional approaches such as radiation shielding and channeling more power to outer lamps result in substantial improvements in temperature uniformity they fail in meeting the stringent requirement of less than 1 °C variation across the substrate required to guarantee the long-term stability of the devices. The problem becomes especially acute while scaling up to larger commercially-viable panel sizes. To this end, a finite element thermal model of a commercial-scale deposition station has been developed and optimized with the target of achieving the desired temperature uniformity of 1 °C. The effects of improvements such as radiation shielding, addition of radiation spreader, contouring of radiation spreader and optimizing power distribution among the radiation lamps have been studied. A new lamp configuration has been proposed for attaining the desired uniformity levels.

Keywords: Photovoltaic cells; Vacuum deposition; IR heating; Thermal modeling and optimization

1. Introduction

Solar energy holds the promise of becoming a cleaner alternative to fossil fuels. Although the price of crystalline silicon solar cells has dropped considerably in past few years [1], even cheaper methods of harnessing solar energy are required in order for it to attain commodity level adoption. To this end, a variety of alternative solar panel technologies such as amorphous silicon, CdTe and Cu(In, Ga)Se_2 are being developed by research groups worldwide [2]. Of these, solar panels fabricated by depositing thin films of cadmium telluride (CdTe) and cadmium sulfide on glass panels have shown a definite potential to replace crystalline silicon [3] as the dominant solar material and a number of processes for developing CdTe solar cells have been developed [4]. So far, the major impediment to successful demonstration of this technology has been the low device stability [5–7]. Recently Sampath and co-workers [8–10] have demonstrated the production of stable CdTe solar panels in their pilot-scale manufacturing facility for 76 mm × 76 mm (3″ × 3″) solar panels. A schematic of this facility is shown in Fig. 1.

The facility is a continuous inline physical vapor deposition system where all the device fabrication steps are performed in one vacuum enclosure. These steps include heating of the glass substrate, deposition of CdS and CdTe films, heat treatment with $CdCl_2$, ohmic contact formation and ohmic contact heat treating. The system is operated at 40 mTorr of N_2. The processing stations are nearly identical in design and construction. Devices produced using the

* Corresponding author. Tel.: +1 303 492 7750; fax: +1 303 492 3498.
E-mail address: mahajan@spot.colorado.edu (R.L. Mahajan).

0017-9310/$ - see front matter © 2006 Elsevier Ltd. All rights reserved.
doi:10.1016/j.ijheatmasstransfer.2006.02.042

Nomenclature

A	area of surface in m^2
C_p	specific heat in J/kg K
F	view factor between surfaces
K	thermal conductivity in W/m K
q	radiation flux incident on surface in W/m^2
T	temperature in °C

Greek symbols

ε	emissivity of surface
ρ	density in kg/m^3
σ	Stefan–Boltzmann constant ($W/m^2 K^4$)

Subscripts

i	surface index for cavity radiation calculations
j	surface index for cavity radiation calculations

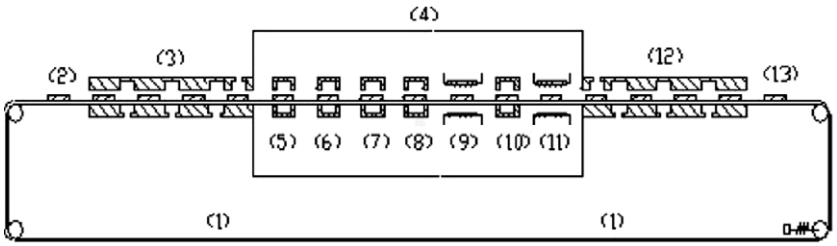

Fig. 1. Schematic of the pilot system for CdTe PV fabrication: (1) belt conveyor, (2) glass substrate, (3) air to vacuum to air (AVA) seal, (4) vacuum chamber, (5) heating module, (6) CdS deposition, (7) CdTe deposition, (8) $CdCl_2$ deposition and heat treatment, (9) $CdCl_2$ annealing and stripping, (10) ohmic contact formation, (11) contact annealing, (12) AVA seal, (13) completed seal.

above pilot system have been subject to accelerated indoor testing and have demonstrated a consistent efficiency of 10.5% over 7500 h of operation. After successful demonstration of the pilot system for manufacturing 76 mm × 76 mm (3″ × 3″) substrates, the facility is being scaled up to produce commercially viable 406 mm × 406 mm (16″ × 16″) panels.

The stability of cells produced by the vapor deposition process is strongly related to the uniformity of deposition of the thin films on the glass substrate [11]. The kinetics of the deposition process being a strong function of temperature, the uniformity of deposition directly depends on the temperature uniformity within the substrates [12,13]. In order to consistently produce stable devices, the variation of temperature across the substrate is to be maintained below 1 °C for a nominal temperature of 500 °C [11]. Simulations show that even without design optimization, the temperature variation within the substrate in the 76 mm × 76 mm (3″ × 3″) pilot facility of Sampath et al. [9] was within 1 °C and hence resulted in the production of stable devices. However, a model of the 406 mm × 406 mm (16″ × 16″) facility shows that the unoptimized variation across the substrate is 17.4 °C which would have a pronounced deleterious effect on the device performance and stability. Hence it was decided to proactively optimize the 406 mm × 406 mm (16″ × 16″) facility to ensure high temperature uniformity before it was employed to manufacture solar panels. The design improvements considered include traditional approaches such as radiation shielding and providing higher power to the outer lamps which are shown to greatly reduce the temperature variation within the substrate but fall short of meeting the target uniformity. A new lamp configuration with optimized power distribution is shown to be effective in reducing the temperature variation across the substrate to the low levels required for manufacturing stable photovoltaic devices.

The paper is organized as follows:

(i) Section 2 outlines the geometry of the deposition station.
(ii) Section 3 gives the details the finite element model and its experimental validation.
(iii) Section 4 presents the simulations and results of the optimization study.
(iv) Section 5 discusses the new lamp configuration to achieve the desired uniformity levels.
(v) Section 6 summarizes the findings of the study.

2. Geometry

The schematic of a 406 mm × 406 mm (16″ × 16″) processing station is shown in Fig. 2. It consists of two identical graphite sources heated by two banks of seven quartz IR lamps. Each source is a 457 mm × 457 mm × 76 mm (18″ × 18″ × 3″) block with a 406 mm × 406 mm (16″ × 16″) central cavity. The cavity in the lower source houses

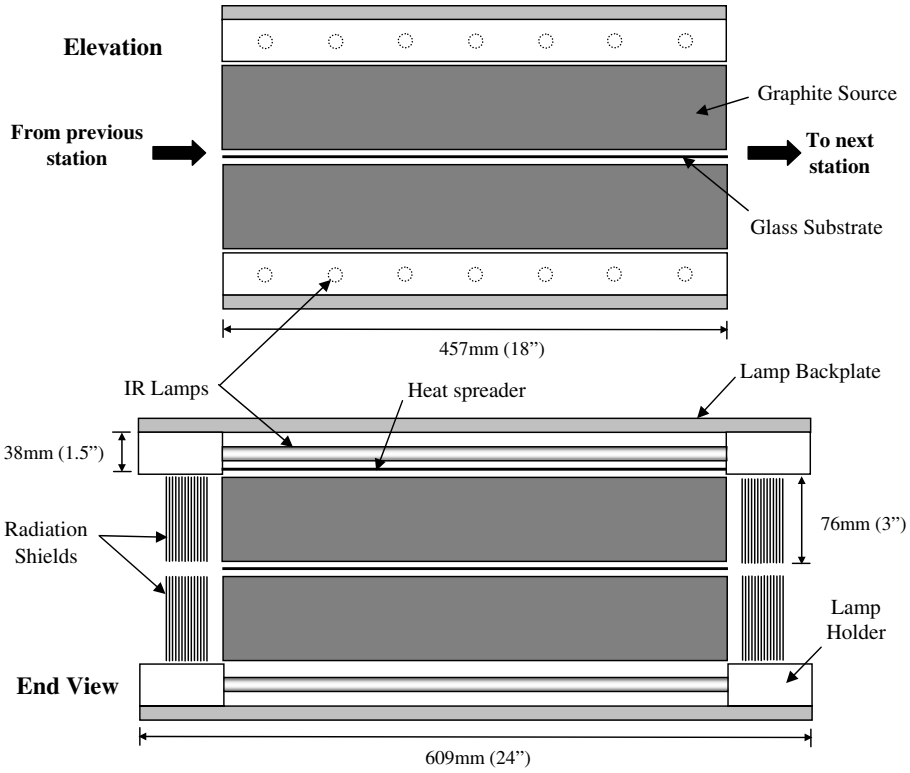

Fig. 2. Elevation and end view of a processing station.

the material to be deposited. The material sublimes and condenses on the underside of a glass substrate placed between the two sources to form the thin-film p–n junction of the solar cell. The IR lamps are housed in lamp holders made of electrically insulating silica material. A stainless steel backplate reflects radiation from the lamps back towards the sources. The end view also shows radiation shields and a heat spreader which will be discussed later in this document.

3. Finite element model

The complexities inherent in the geometry and the nonlinear property variation preclude accurate quantification of the uniformity using analytical approaches. Hence, the finite element approach was employed to develop the thermal model of the station. Since the transport processes in the current study occur in near vacuum, it is assumed that heat transfer within the system only takes place by radiation exchange between the exposed surfaces and by conduction through the solid sections. The nonlinear finite element software ABAQUS was selected for developing the model since it has a built-in solver for cavity radiation and permits the solution of coupled transient radiation–conduction problems with nonlinear property variation. Since the geometry is symmetric about midplanes in all three Cartesian directions, only 1/8th of the geometry needs to be modeled by assigning symmetry boundary conditions along the midplanes.

Bounding surfaces were added to the top, back and side of the model to represent the vacuum chamber and provide boundary conditions for cavity radiation. Bounding surfaces on the top and back were assigned a uniform temperature of 70 °C which is representative of values measured in the chamber walls of the pilot scale system. It is to be noted that in the actual setup, each station will have similar stations adjacent to it on its two sides. Since the current model is representative of any given station it is assumed that the adjacent station is at a temperature not much different from the current station. Hence, a zero flux or symmetry boundary condition is applied to the surfaces on the side of the model.

The model is meshed using a combination of shell and brick heat transfer elements. Since the length to thickness ratio of the substrate is very large, to prevent loss of accuracy associated with high aspect ratio solid elements or an inordinately fine mesh dictated by the small thickness of the substrate, the substrate was meshed using four noded shell elements which account for temperature variations in the thickness direction by numerical integration. The lamps too were meshed as 2.54 mm (0.1″) thick hollow shells to closely represent the actual geometry of the IR quartz lamps being used. All the other components (except the radiation shields and the heat spreader) shown in Fig. 2 were meshed using solid eight noded heat transfer brick elements. Temperature dependent properties were supplied for all materials in the model. These are summarized in Tables A.1–A.5 in Appendix.

The cavity radiation formulation in ABAQUS is based on the gray body assumption with diffuse reflection [14]. Each exposed face of an element is considered as an isothermal, isoemissive surface. The emissivities assigned to the various materials considered in the model are given in Table A.6 in Appendix. View factors between individual facets are calculated using the basic formula,

$$F_{ij} = \int_{A_i} \int_{A_j} \frac{\cos\phi_i \cos\phi_j}{\pi R^2} \, \mathrm{d}A_i \, \mathrm{d}A_j$$

where, $\mathrm{d}A_i$ and $\mathrm{d}A_j$ are the areas of the facets, R is the distance between their centers and ϕ_i, ϕ_j are the angles between the line connecting the centers of the two facets and their respective normals. The view factor calculation algorithm in ABAQUS also takes into account general surface blocking (or shadowing) as well as the most common forms of radiation symmetry. The current model uses the planar symmetry module in ABAQUS across the three Cartesian directions. The cavity radiation flux entering each facet of the cavity is calculated using the formula,

$$q_i = \frac{\sigma \varepsilon_i}{A_i} \sum_j \varepsilon_j \sum_k F_{ik} C_{kj}^{-1} \left((T_j + 273.15)^4 - (T_i + 273.15)^4 \right)$$

where

$$C_{ij} = \delta_{ij} - \frac{(1 - \varepsilon_i)}{A_i} F_{ij}$$

and δ_{ij} is the Kronecker delta. The cavity radiation flux is converted into nodal fluxes and applied to the exposed nodes.

To simulate heating from the IR lamps, a surface flux was applied to the outer surface of the lamp shells. The magnitude of the surface flux multiplied by the total surface area of the lamps was taken as the power input to the lamps. The steady-state solver in ABAQUS was invoked and the solution was assumed to be converged when the maximum residual heat flux in the model was below 0.5%. Each calculation took approximately 3 h. When the mesh was refined by approximately 1.5 times the maximum difference in temperature at points of interest in the source and substrate changed by only 0.3% while the computational time increased to 15 h. Since the changes in temperature were within 1% while the increase in computational time was approximately 5-fold, the basic mesh was used in this study. A mesh refinement of over 1.5 times exceeded the 3GB memory capacity of the machine and could not be attempted.

Experimental trials were conducted on an actual processing station similar to the one shown in Fig. 2. The power input to the bottom lamps was adjusted to bring the temperature at the center of the pocket in the bottom source to approximately 400 °C. With the temperature in the center of the pocket at ~400 °C, the temperatures at the rear and side of the pocket as well as that at the center of the top source were recorded. The experiment was carried out for two configurations: (i) without any radiation shields on the top source and (ii) with radiation shields on the periphery of the top source. These two experiments were simulated using the finite element method described above. A comparison of the results from the two experiments and the corresponding values from the finite element model is given in Table 1. As seen from the table, the predictions of the model are within about 1% of the experimental data. The good agreement between the predictions of the finite element model and the experimental data established the validity of the modeling approach and the thermophysical properties used, in capturing the thermal transport in the actual system. Hence the modeling approach was used further for optimizing the processing station for minimum temperature variation within the substrate.

Table 1
Comparison of predictions of finite element model with experimental results

	Bottom source				Top source
	Center	Side	Rear	Corner	Center
Experiment (with top shields)	399	386	391	384	224
Finite element model	399	389.6	393.8	386.5	226.7
Error (%)		0.9	0.7	0.6	1.2
Experiment (without top shields)	401	–	394	388	267
Finite Element Model	401	391.4	396.4	389.6	264.4
Error (%)		–	0.6	0.4	1.0

4. Simulations and optimization

Using the configuration shown in Fig. 2, simulations were carried out to get the unoptimized temperature variation within the substrate. The lamp power was adjusted to obtain a target temperature of 500 ± 0.3 °C at the center of the substrate. The largest temperature difference in the substrate is obtained between the center and the corner and was found to be 17.4 °C. This is the baseline unoptimized temperature variation over which improvements were sought. The unoptimized power consumption was 2 kW.

Three methods traditionally used in the vacuum industry for reducing temperature variation were successively applied to the unoptimized geometry in order to improve the temperature uniformity within the substrate. First, radiation shields were added to the front and back of the source in order to prevent heat loss from the source to the chamber walls and thereby improve the uniformity within the source. Since the substrate is in very close proximity to the sources and gets heated via radiation from them, it can be expected that a reduction in temperature variation within the source would result in a corresponding reduction in temperature variation within the substrate. Second, a radiation spreader was added between the lamps and source to distribute the heat from the lamps uniformly to the top surface of the source. The spreader geometry itself could be optimized for maximizing uniformity.

Finally, the lamps could be wired separately and the power distribution across the lamps could be changed to obtain an optimum power distribution across the lamps which results in the maximum uniformity. The results of applying these three methods for improving the thermal uniformity are presented below.

4.1. Addition of radiation shields

Radiation shields in the form of 1 mm (0.04″) thick stainless steel plates were added at the back of the source as shown in Fig. 2. The dimensions of the radiation shields were same as those of the face of the source and they were placed at a distance of 1.5 mm (0.06″) from each other. Due to the large length to thickness ratio of the shields, as with the substrate, they too were meshed with four noded shell elements.

Since the shields were located in close proximity to each other, it was assumed that the view factor between adjacent radiation shields was 1 and hence the simpler gap radiation formulation in ABAQUS was applied to the spaces between the radiation shields which is given by the standard formula,

$$q = \frac{\sigma((T_A + 273.15)^4 - (T_B + 273.15)^4)}{1/\varepsilon_A + 1/\varepsilon_B - 1}$$

where the suffixes A and B represent two adjacent shields.

For a given value of power supplied to the lamps, with every additional radiation shield, the substrate temperature increased due to the lowering of heat loss from the sources. The power supplied to the lamps was incrementally reduced till the temperature at the center of the substrate was brought back to 500 ± 0.3 °C. The difference between the maximum and minimum temperatures within the substrate was recorded as the maximum temperature variation within the substrate. This variation was plotted as a function of number of radiation shields and is shown in Fig. 3. The power required to maintain the substrate at 500 °C with the addition of radiation shields is also shown in Fig. 3.

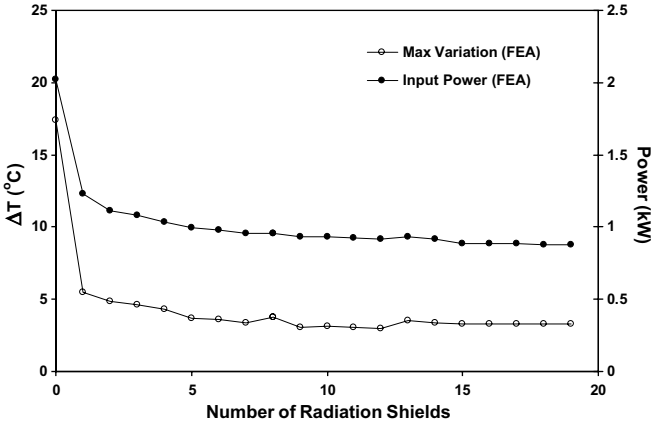

Fig. 3. Change in maximum temperature variation in substrate and power required to maintain temperature at the center of the substrate at 500 ± 0.3 °C with number of radiation shields.

Two important deductions can be made from Fig. 3. First, the addition of a single shield results in the maximum reduction in power input and also results in the maximum decrease in temperature variation from 17.4 °C to 5.5 °C. The relative improvement with additional shields is small and beyond 15 shields, the incremental reduction in power or temperature variation is negligible. The configuration with 15 radiation shields was therefore accepted as optimum at which the maximum temperature variation within the substrate was 3.3 °C and the power consumption was 0.89 kW. In conclusion, the addition of radiation shielding results in a significant drop in temperature variation from 17.4 °C to 3.3 °C.

4.2. Addition of radiation spreader

In order to further decrease the temperature variation within the substrate, a radiation spreader in the form of a 3.2 mm (1/8″) stainless steel plate was added between the lamps and the source as shown in Fig. 2. It was theorized that adding the spreader would provide a more uniformly distributed source of heat addition as opposed to the discrete lamps and also serve to reduce heat loss from the top edges of the source to the lamp holder. However, the effect of the heat spreader was not very large. Its addition reduced the maximum temperature variation within the substrate from 3.3 °C to 2.7 °C while the power consumption increased from 0.89 kW to 0.92 kW.

Next, we sought to optimize the spreader geometry to see if any further improvements in uniformity could be obtained. Changing the thickness of the spreader from 3.2 mm (1/8″) to 6.4 mm (1/4″) resulted in no significant improvement in the temperature variation (only 0.05 °C). The effect of using a spreader area smaller than the source area was studied next. The motivation behind contouring the spreader was to direct more heat towards the back of the source from where the main heat loss takes place. Fig. 4 shows the effect of increasing the gap between the edge of the spreader and the heater holder. As can be seen from the figure, the curve shows a minimum at a gap of 76.2 mm (3″). However, the difference between the minimum temperature difference (2.64 °C) and the temperature difference with a full spreader (2.67 °C) is again insignificant. Moreover, decreasing the spreader width on the sides always resulted in increase in the temperature variation within the substrate. Hence, it was concluded that contouring the spreader provides no significant benefit over the use of a spreader that completely shields the lamps from the source. The reason for this lack of improvement was due to the fact that though the a gap on the back of the source directed incrementally more radiative flux there, it also exposed the top edges of the source directly to the heater holder to which they lost heat. These effects balance at the optimum spreader gap of 76.2 mm (3″) but no overall improvement is obtained.

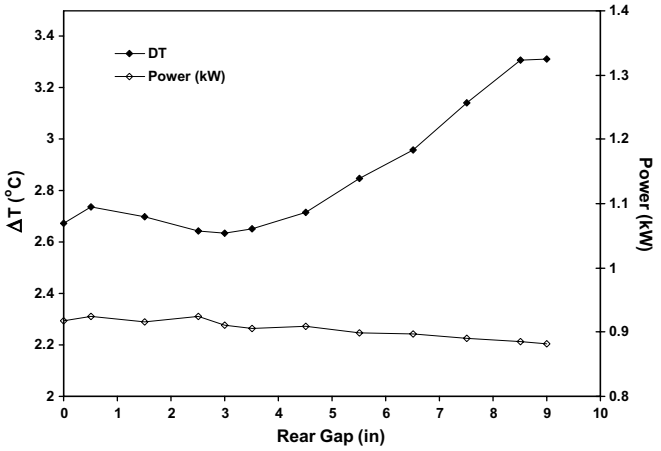

Fig. 4. Variation in maximum temperature difference within substrate and input power with gap between heater holder and edge of spreader.

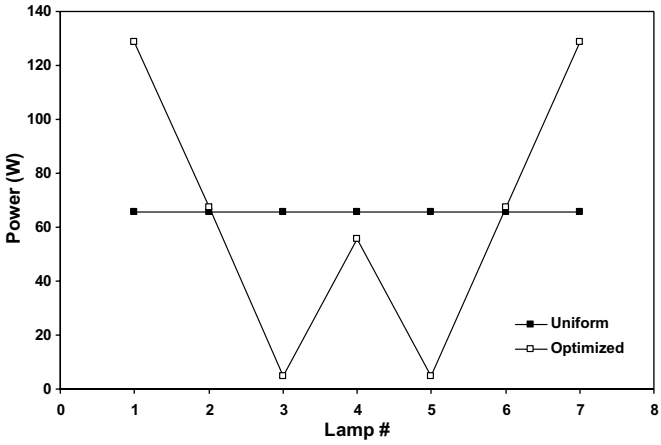

Fig. 5. Unoptimized and optimized lamp power distributions.

4.3. Optimum power distribution among lamps

A common method in obtaining temperature uniformity in rapid thermal processing (RTP) systems is to individually control the power input to each heating lamp [15–22]. This approach was adopted here to further improve the temperature uniformity within the substrate. In order to find the power input to each lamp so that the maximum possible uniformity would be realized, an optimization program DN0ONF from the mathematical library IMSL [23] was interfaced to ABAQUS. This program is based on a FORTRAN subroutine NLPQL developed by Schittkowski [24] and employs the successive quadratic programming method to solve general constrained nonlinear programming problems. To find the optimum power distribution, this problem was specified as

minimize $f(x_i)$

where

$f(x_i) = T_{\text{substrate-max}} - T_{\text{substrate-min}}$

and x_i's are power inputs to individual lamps subject to,

$|T_{\text{substrate-mid}}\text{-}500| \geqslant 0.3$

and

$0 \leqslant x_i \leqslant 50$

The maximum lamp flux was limited to 50 W/in.^{2} corresponding to the maximum output of 1500 W per lamp. The equality constraint on the temperature at the center of the substrate was converted to the inequality constraint with a tolerance of ± 0.3 °C to speed up the optimization process. Each evaluation of $f(x_i)$ required one simulation in ABAQUS. Since most of the computational effort in a simulation was consumed in the calculation of view factors which did not change in this part of the study, an interfacing program was written which updated the lamp fluxes and obtained the substrate temperatures without exiting the ABAQUS run; the interfacing program then used reverse communication to update the work function and constraints in the optimizer.

The unoptimized and optimum lamp power distributions are shown in Fig. 5. The optimization of the lamp powers for maximizing uniformity at a nominal temperature of 500 °C resulted in reduction of the maximum temperature variation within the substrate from 2.7 °C to 2.5 °C and the total power consumption remained unchanged at 0.92 kW. Even after optimizing the power distribution to the lamps, only a slight improvement in uniformity was obtained. This indicated that the heating configuration shown in Fig. 2 was inherently inadequate in meeting the target temperature variation of below 1 °C required for producing stable thin film photovoltaics and a change in lamp configuration was necessary to obtain further improvement in uniformity. Hence a new lamp configuration was sought.

5. New lamp configuration

In order to gain insight into the effect of various improvements discussed above on the temperature variation within the substrate, the temperature contours within the substrate were plotted and are presented in Fig. 6. As can be seen from the figure, in the unoptimized configuration, the temperature within the substrate rapidly decreases from 500 °C at the center to 482.6 °C at the corner. Addition of radiation shields substantially prevents heat loss from the front and back of the source thus significantly improving the uniformity within the substrate. The maximum and minimum temperatures yet occur at the center and corner respectively. Addition of a spreader between the lamps and the source serves to reduce the temperature gradients within the substrate. Optimization of power distribution among the lamps directs the power to the outer lamps which moves the location of the maximum temperature from the center of the substrate to the side of the substrate. This serves to direct the majority of the heat flow through the radiation shields as opposed to the corner of

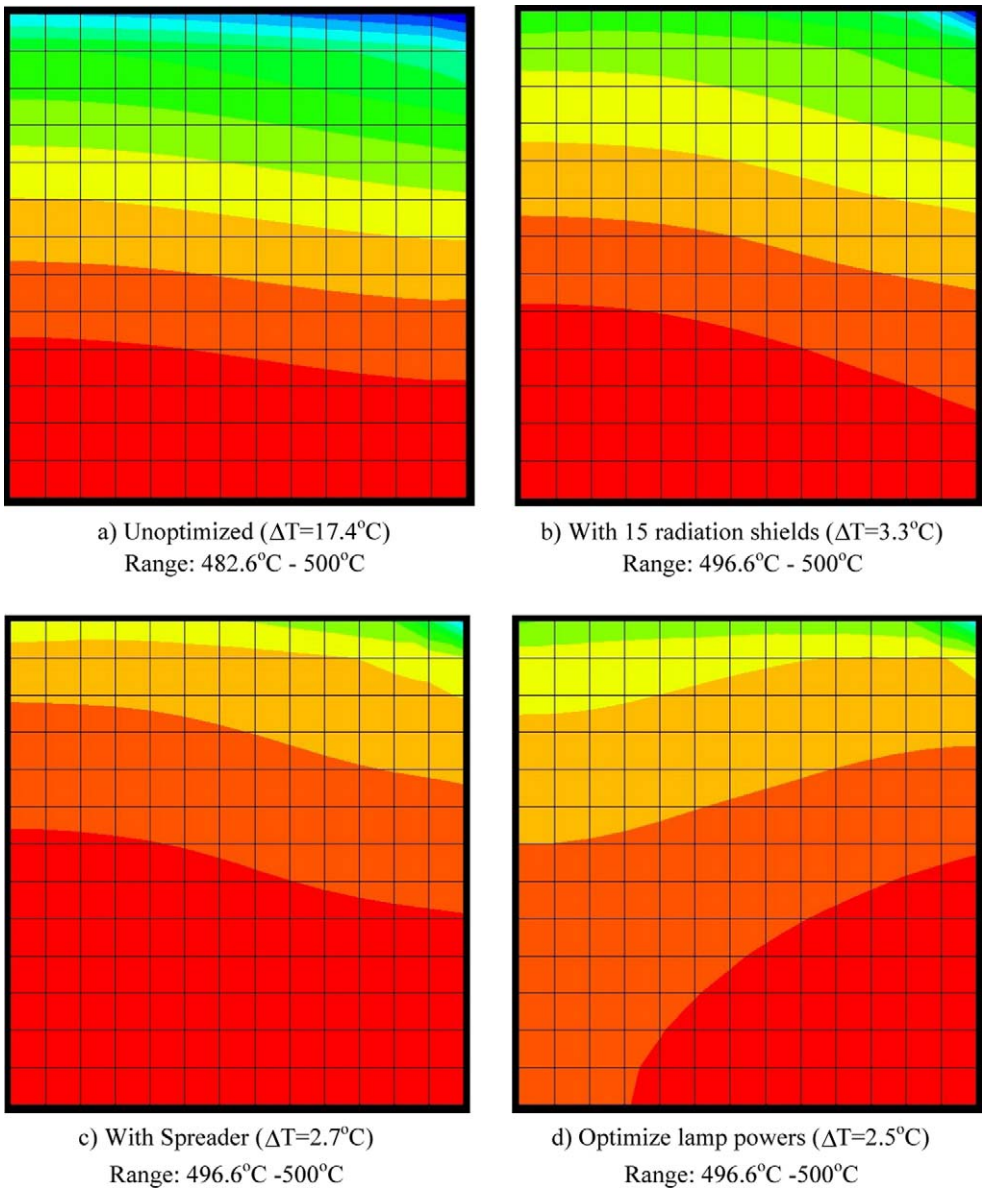

Fig. 6. Temperature contours within substrate with increasing uniformity.

the source thereby further reducing the temperature variation. The above temperature contours indicate that further improvement in uniformity can only be obtained by actively restricting the heat flow from the front and back of the source. Passive shields can only achieve this up to a point. Hence, it was decided to place an active source of heat i.e. an IR lamp instead of the radiation shields in front and back of the source as shown in Fig. 7.

Three different optimization studies were undertaken after adding the extra lamp at the front and back of the sources. In the first study, all the lamps were assigned the same amount of power. This is the easiest configuration from an ease-of-control perspective. With all lamps drawing the same power, the maximum temperature variation was found to be 2.6 °C which is only marginally better than 2.7 °C obtained for the case with radiation shields, no front and back lamps, and uniform power distribution among top and bottom lamps. The total power consumption however increased from 0.92 kW to 1.35 kW. In the second study, the top and bottom lamps were assigned the same power while the front and back lamps were assumed to be controlled independent of them. In this case, the maximum variation within the substrate dropped to 1.2 °C while the overall power consumption increased to 1.42 kW. Out of this only 0.61 kW was consumed by the 14 top and bottom lamps while the rest (0.81 kW) was consumed by the four front and back lamps. The uniformity so obtained was within reach of the target of 1 °C. In the last study, the power supply to every lamp was varied independently. This resulted in a maximum variation of only 0.65 °C. The total power drawn by the system was 1.42 kW. Of this the optimizer directed 0.75 kW to the four

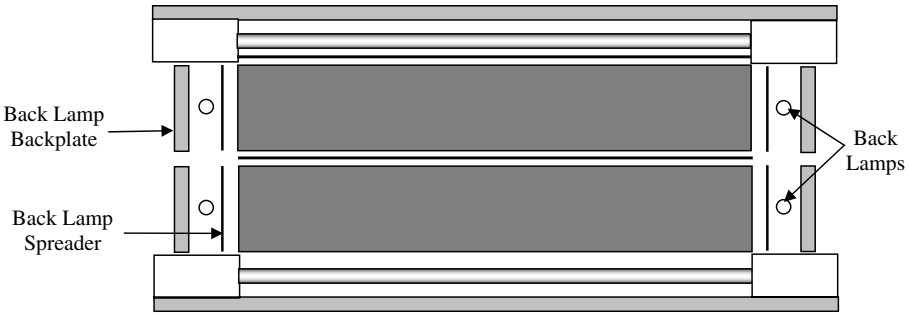

Fig. 7. Schematic showing location of back lamp assembly.

front and back lamps, 0.6 kW to the four edge lamps in the top and bottom and a small amount (0.06 kW) to the two middle lamps in the top and bottom. The rest of the lamps i.e. the inner lamps in the top and bottom with the exception of the middle lamps drew no power. Thus it can be concluded that the inner lamps in the top and bottom are

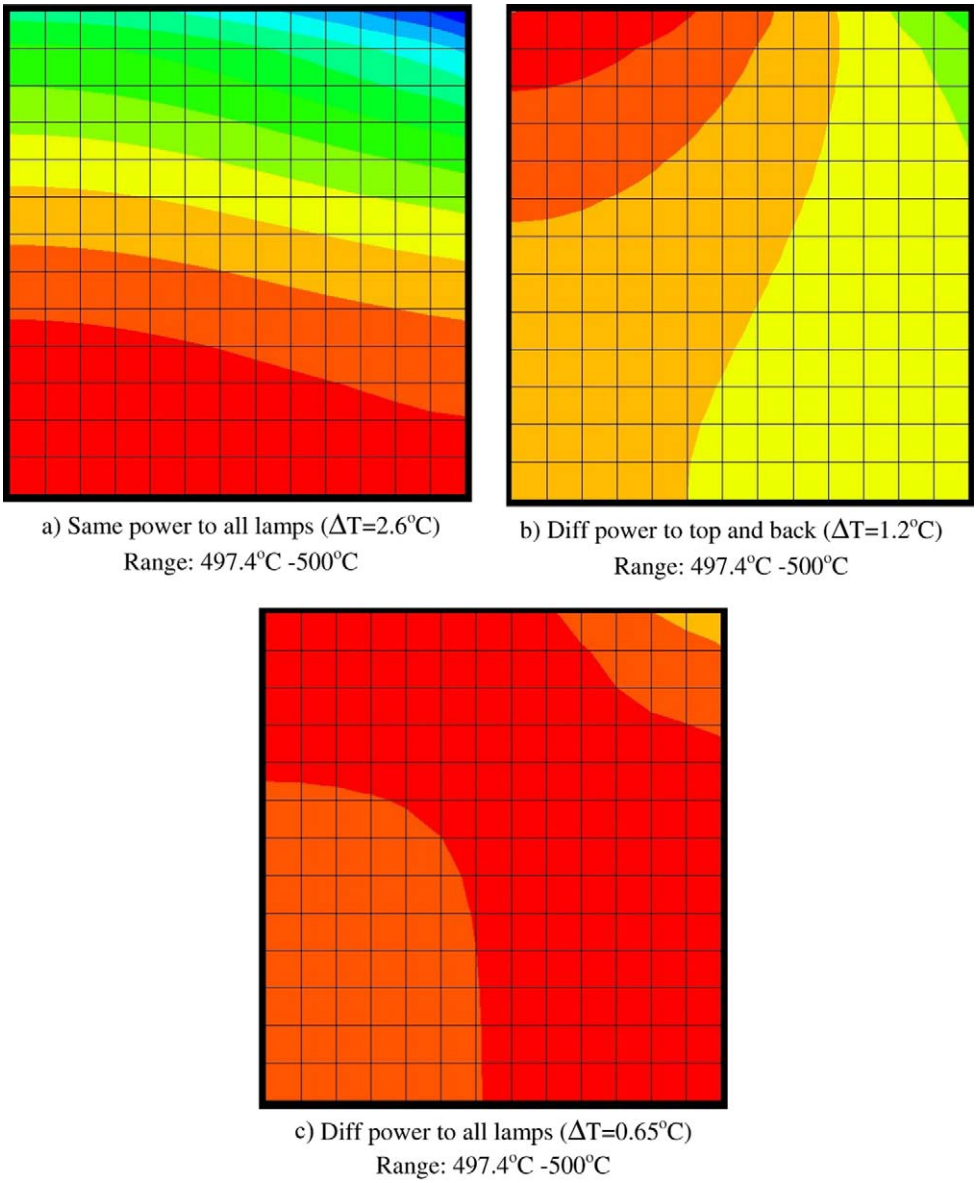

Fig. 8. Temperature contours within substrate for three optimization studies with front and back lamps instead of radiation shields.

redundant i.e. effective heating and control of thermal uniformity within the substrate can be obtained by only the four edge lamps on the top and bottom of the sources and the 4 lamps in the front and back of the two sources.

The temperature contours obtained within the substrate in the above three studies are presented in Fig. 8. The general nature in temperature contours is largely unchanged between Figs. 6c and 8a and the temperature uniformity is almost identical in both cases indicating that though the addition of front and back lamps can be an impediment to heat flow from the front and back surfaces of the sources (as was the case with the radiation shields for Fig. 6c), the constraint that they have the same power as the top lamps is too restrictive and does not alter the general nature of heat flow in the problem. Fig. 8b shows a considerable departure from the general problem in that it shows that heating from the front and back lamps is preferable to heating from the top and bottom lamps for achieving higher thermal uniformity within the substrate. This is also concluded from the fact that a majority of the power is directed to the front and back lamps as opposed to the top and bottom lamps. Lastly Fig. 8c shows that the most optimized heating configuration for the current problem distributes power to the front and back lamps and the outer or edge lamps in the top and bottom banks thus providing the most symmetric temperature distribution within the substrate permitted by the problem.

6. Summary

The fabrication of stable thin film CdTe photovoltaic cells necessitates tight control of temperature uniformity within the substrate during the vacuum deposition process. Though the configuration for producing 76 mm × 76 mm (3″ × 3″) panels meets these uniformity requirements, on scaling the panel size to 406 mm × 406 mm (16″ × 16″) it is no longer possible to achieve the desired uniformity levels even after employing traditional methods such as radiation shielding and directing more power to the outer lamps. Hence it is necessary to employ computer based optimization techniques for maximizing the temperature uniformity. To this end, a finite element model of a single processing station was developed, interfaced to a numerical optimization routine in IMSL, and the effect of various uniformity enhancement techniques was studied. The findings of the study are summarized in Table 2. It can be concluded that while passive shielding and optimizing the power distribution to different lamps can substantially improve the thermal uniformity in the substrate, they cannot alter the basic heat flow patterns in the graphite sources and thus a temperature gradient always exists between the center and the rear of the sources. Addition of an active heat source (IR lamps) in the front and back of the graphite sources and then optimizing the power input to all the lamps results in a heat flow pattern that directs heat from the peripheral lamps towards the center of the source and results in a maximum variation of only 0.65 °C within the substrate which is well within the target value of 1.0 °C. The optimization study also indicates that the inner lamps in the top and bottom banks are redundant and can be safely removed without loss in thermal uniformity.

Table 2
Summary of findings of optimization study

Configuration	Max temperature variation in substrate (°C)	Total power consumption (kW)
Basic	17.4	2.00
Add 15 radiation shields	3.3	0.89
Add spreader	2.7	0.92
Optimize spreader geometry	2.6	0.91
Optimize power distribution among lamps	2.5	0.92
Add front and back lamps (remove shields) same power to all lamps	2.6	1.35
Different power levels to top/bottom and front/back lamp banks	1.2	1.42
Different power levels to all lamps	0.65	1.42

Acknowledgement

The authors gratefully acknowledge the partial funding extended by the International Center for Science and High Technology (ICS), Trieste, Italy.

Appendix. Thermophysical properties of materials used in finite element model

Tables A.1–A.6.

Table A.1
Properties of graphite sources [25]

T (°C)	K (W/m K)	T (°C)	C_p (J/kg K)	ρ (kg/m^3)
0	110	26.85	721.4	1700
200	85	76.85	875	
400	72	126.85	1025.8	
600	62	176.85	1155.6	
800	55	226.85	1268.6	
1000	50	276.85	1352.3	
1200	45	326.85	1423.5	
1400	41	376.85	1490.5	
1600	38	426.85	1549.2	
		476.85	1599.4	
		526.85	1645.4	
		576.85	1683.1	
		626.85	1712.4	
		676.85	1737.5	
		726.85	1762.6	
		826.85	1808.7	
		926.85	1854.7	
		1026.85	1892.4	

Table A.2
Properties of stainless steel [26]

T (°C)	K (W/m K)	C_p (J/kg K)	ρ (kg/m^3)
−73.15	12.6	402	7900
126.85	16.6	515	
326.85	19.8	557	
526.85	22.6	582	
726.85	25.4	611	
926.85	28	640	
1226.85	31.7	682	

Table A.3
Properties of soda lime glass [27]

T (°C)	K (W/m K)	C_p (J/kg K)	ρ (kg/m^3)
20.85	1.2	936.32	2530
41.85	1.48		
88.85	1.38		
126.85	1.56		
157.85	1.62		
202.85	1.74		
244.85	1.85		
270.85	1.74		

Table A.4
Properties of quartz lamps [28]

T (°C)	K (W/m K)	T (°C)	C_p (J/kg K)	ρ (kg/m^3)
0	1.44	−17.14	520	2200
98.77	1.60	41.63	660	
209.88	1.73	106.94	767	
320.99	1.84	185.31	867	
432.10	1.90	263.67	947	
506.17	1.93	361.63	1020	
623.46	1.93	518.37	1060	
765.43	1.93	609.80	1080	
895.06	1.94	727.35	1107	
		838.37	1133	
		936.33	1160	
		995.10	1180	
		1112.65	1220	

Table A.5
Properties of silica insulator [29]

T (°C)	K (W/m K)	C_p (J/kg K)	ρ (kg/m^3)
20.85	1.2	936.32	2530
41.85	1.48		
88.85	1.38		
126.85	1.56		
157.85	1.62		
202.85	1.74		
244.85	1.85		
270.85	1.74		

Table A.6
Emissivities assigned to the various materials in the finite element model

Material	Emissivity	Reference
Graphite	0.8	[25]
Stainless steel	0.25	[26]
Soda lime glass	0.8	[27]
Quartz lamps	1.0	–[a]
Silica	0.5	[30][b]

[a] The lamps were assumed to radiate out all the heat flux applied on their outer surface.

[b] Since the spectral emissivity of silica as reported by Rozenbaum et al. [30] varies rapidly from 1 to 0 in the wavelengths corresponding to thermal radiation, an average value of 0.5 was used.

References

[1] D. Mooney, R. Mitchell, E. Witt, R. King, D. Ruby, PV Manufacturing R&D accomplishments and status, Technical Report, NREL/TP-520-35278, National Renewable Energy Laboratory, 2003.

[2] K. Zweibel, Harnessing Solar Power: The Photovoltaics Challenge, Perseus Publishing, 1990.

[3] D. Bonnet, P. Meyers, Cadmium telluride—material for thin film solar cells, J. Mater. Res. 13 (10) (1998) 2740–2753.

[4] D. Bonnet, The CdTe thin film solar cell—an overview, Int. J. Sol. Energy 12 (1992) 1–14.

[5] I. Visoly-Fisher, K.D. Dobson, J. Nair, E. Bezalel, G. Hodes, D. Cahen, Factors affecting the stability of CdTe/CdS solar cells deduced from stress tests at elevated temperature, Adv. Funct. Mater. 13 (4) (2003) 289–299.

[6] K.D. Dobson, I. Visoly-Fisher, G. Hodes, D. Cahen, Stability of CdTe/CdS thin-film solar cells, Sol. Energy Mater. Sol. Cells 62 (3) (2000) 295–325.

[7] T.K. Brog, Commercial production of thin-film CdTe photovoltaic modules, Technical Report, NREL/SR-520-23733, National Renewable Energy Laboratory, 1997.

[8] K.L. Barth, R.A. Enzenroth, W.S. Sampath, Advances in continuous, in-line processing of stable CdS/CdTe devices, in: Proceedings of the Twenty-Ninth IEEE Photovoltaic Specialists Conference, New Orleans, LA, 2002, pp. 551–554.

[9] W.S. Sampath, K.L. Barth, R.A. Enzenroth, Continuous, in-line processing of stable CdS/CdTe devices, in: Proceedings of the NCPV Program Review Meeting, Lakewood, CO, 2001.

[10] K.L. Barth, R.A. Enzenroth, W.S. Sampath, Apparatus and processes for the mass production of photovoltaic modules, US Patent No. 6423565, 2002.

[11] W.S. Sampath, National CdTe R&D Team Meeting Minutes, unpublished, 2004.

[12] T.L. Chu, Cadmium telluride solar cells, in: T.J. Coutts, J.D. Meakin (Eds.), Current Topics in Photovoltaics, Academic Press, New York, 1988, pp. 235–300.

[13] R.L. Mahajan, Transport phenomena in chemical vapor deposition systems, Adv. Heat Transfer 28 (1996) 339–425.

[14] ABAQUS Online Documentation v.6.4.1: Copyright 2003, ABAQUS, Inc.

[15] R.S. Gyurcsik, T.J. Riley, F.Y. Sorrell, A model for rapid thermal processing: achieving uniformity through lamp control, IEEE Trans. Semicond. Manuf. 4 (1) (1991) 9–13.

[16] F.Y. Sorrell, M.J. Fordham, M.C. Öztürk, J.J. Wortman, Temperature uniformity in RTP furnaces, IEEE Trans. Electron Dev. 39 (1) (1992) 75–80.

[17] S.A. Norman, Optimization of transient temperature uniformity in RTP systems, IEEE Trans. Electron Dev. 39 (1) (1992) 205–207.

[18] Y.M. Cho, A. Paulraj, T. Kailath, G. Xu, A contribution to optimal lamp design in rapid thermal processing, IEEE Trans. Semicond. Manuf. 7 (1) (1994) 34–41.

[19] K.L. Knutson, Modeling of three-dimensional effects on temperature uniformity in rapid thermal processing of eight inch wafers, IEEE Trans. Semicond. Manuf. 7 (1) (1994) 68–72.
[20] R.H. Perkins, T.J. Riley, R.S. Gyurcsik, Thermal uniformity and stress minimization during rapid thermal processes, IEEE Trans. Semicond. Manuf. 8 (3) (1995) 272–279.
[21] J. Dilhac, N. Nolhier, C. Ganibal, C. Zanchi, Thermal modeling of a wafer in a rapid thermal processor, IEEE Trans. Semicond. Manuf. 8 (4) (1995) 432–439.
[22] S. Lin, H. Chu, Thermal uniformity of 12-in silicon wafer in linearly ramped temperature transient rapid thermal processing, IEEE Trans. Semicond. Manuf. 14 (2) (2001) 143–151.
[23] IMSL Math Library, Vol. 3.0: Copyright 1997, Visual Numerics, Inc.
[24] K. Schittkowski, NLPQL: a FORTRAN subroutine solving constrained nonlinear programming problems, Ann. Oper. Res. 5 (1986) 485–500.
[25] R.G. Sheppard, D.M. Mathes, D.J. Bray, Properties and Characteristics of Graphite, Poco Graphite, Inc., 2001.
[26] F.P. Incropera, D.P. DeWitt, Fundamentals of Heat and Mass Transfer, third ed., John Wiley & Sons, New York, 1990. Appendix A.
[27] Y.S. Touloukian (Ed.), Thermophysical Properties of Matter—The TPRC Data Series, IFI/Plenum, New York, 1970.
[28] GE quartz: thermal properties, Copyright 1997–2002, General Electric Company. <http://www.gequartz.com/en/thermal.htm>, 2004 (accessed 04.05.04).
[29] Zircar, Refractory sheet type RSLE-57—properties & characteristics, Copyright Zircar Refractory Composites, Inc. <http://www.zrci.com/rsle-57.htm>, 2004 (accessed 04.05.04).
[30] O. Rozenbaum, D. De Sousa Meneses, Y. Auger, S. Chermanne, P. Echegut, A spectroscopic method to measure the spectral emissivity of semi-transparent materials up to high temperature, Rev. Sci. Instrum. 70 (10) (1999) 4020–4025.